

# Novel Fracton Phases from Gauge Theories

J. P. Ibieta-Jimenez,<sup>\*</sup> L. N. Queiroz Xavier,<sup>†</sup> and P. Teotonio-Sobrinho<sup>‡</sup>

*Departamento de Física Matemática, Universidade de São Paulo,  
Rua do Matão Travessa R 187, CEP 05508-090, São Paulo, Brazil.*

(Dated: August 22, 2019)

We introduce new models of fracton order based on  $\mathbb{Z}_2$  lattice gauge theories in  $d = 2$  and  $d = 3$  spatial dimensions. In the  $3d$  models, the ground state degeneracy grows exponentially with the square of the linear size of the system at the same time as it exhibits a dependence on the topology of the underlying manifold. Also, there are completely mobile gauge charges living along with immobile fractons. Until now most fracton models were obtained from a process of gauging subsystem symmetries of some generalized Abelian lattice gauge theories, and our method shows that fracton phases are also present in more usual lattice gauge theories. We also show how to construct fracton models from lattice gauge theories with arbitrary, possibly non-Abelian finite gauge groups and as examples, we study fracton models obtained from choosing  $\mathbb{Z}_3$  and  $S_3$  as gauge groups.

## I. INTRODUCTION

Since the discovery of the fractional quantum Hall (FQH) effect [1, 2], it is known that there are quantum phases of matter that cannot be explained by Landau's symmetry breaking theory. Topologically ordered phases, of which FQH states are a standard example, encompass phases that are beyond the scope of Landau's theory. Intrinsic topological order can be characterized as exhibiting, among other properties, a ground state degeneracy that depends on the topology of the underlying space in which the system lives [3] and long-range entangled ground states [4], which means that they cannot be transformed into product states by means of local unitary transformations. Another important feature of topological phases is the presence of anyonic excitations, which is essential to the potential application of topological order in fault-tolerant quantum computation [5, 6]. A classical example of intrinsic topological order is Kitaev's toric code [5], first introduced in the context of quantum computation as a quantum error correction code and as a way of implementing a quantum memory. This model can be interpreted as a  $\mathbb{Z}_2$  lattice gauge theory, and it is a particular case of a larger class of models known as quantum double models [5, 7–9], which are topologically ordered exactly solvable models based on lattice gauge theories with arbitrary finite gauge groups.

It is also possible to have topological order with short-range entanglement of the ground states if there are global symmetries in the system. Phases with such behavior are known as symmetry protected topological (SPT) phases [10, 11], and they are characterized by the fact that entangled ground states cannot be transformed into non-entangled ones by means of local unitary transformations without breaking a global symmetry. The

classification of SPT phases is known to be related to the group cohomology of the global symmetry group [11, 12].

Intrinsic topological order has its low-energy behavior described by topological quantum field theories (TQFTs), which are intimately connected to category theory [13]. In particular, string-net models [14], a more general framework that captures essential features of topological phases in  $d = 2$  spatial dimensions, are obtained from fusion categories. It is becoming clear that, for systems in  $d > 2$  dimensions, higher category theory and higher gauge theory [15, 16] are essential to understand topological order. A variety of models of topological phases obtained from these structures can be found in the literature [17–20].

Recently, it was theorized that a new type of quantum phase of matter lies beyond the topological order framework. The so-called fracton order [21–23] refers to quantum phases of matter in which distinct ground states cannot be distinguished by local measurements, a feature shared with topologically ordered systems. However, the ground state degeneracy exhibits a subextensive dependence on the system size, in contrast with the constant ground state degeneracy of topologically ordered models. Also, the spectrum of fracton models is composed by quasi-particles with several mobility restrictions, and some of the excitations, the so-called fractons, are completely immobile, i.e., cannot be moved by string-like operators, in contrast with anyons in topologically ordered models which are free to move around the lattice.

Based on the mobility of its excitations, it is common to divide gapped fracton phases into two distinct types: in type-I fracton phases, immobile fractons appear at the corners of membrane-like operators, and there are other quasi-particles that can move along sub-dimensional manifolds, for example along lines or planes if the system is 3-dimensional. In type-II fracton phases, the only excitations are completely immobile fractons and they live at the corners of fractal-like operators. Standard examples of models exhibiting type-I and type-II fracton phases are the X-cube model [22, 24] and the Haah code [25], respectively. Both are exactly solvable

---

<sup>\*</sup> pibieta@if.usp.br  
<sup>†</sup> lucasnix@if.usp.br  
<sup>‡</sup> teotonio@if.usp.br

spin models in  $d = 3$  dimensions. Gapped fracton models are related to glassy physics and localization [21, 26–30] and they present potential applications to quantum information [25, 31–37]. There are also gapless fracton models arising from the study of symmetric tensor gauge theories [38–43]. This approach allows a connection of fracton models with elasticity theory and gravity [44–46], and some gapped fracton phases can be obtained from symmetric tensor gauge theories defined on the lattice by a Higgs mechanism [41, 47]. The relation between gapless fracton phases and gravity suggests that fracton models may be considered as toy models for the holographic principle [48].

There are ways of generating fracton phases from known topologically ordered models. For example, the X-cube model can be obtained by coupling layers of 2-dimensional toric codes [42, 49, 50]. However, the most common manner in which fracton models are obtained is by considering lattice spin systems with subsystem symmetries as generalized Abelian lattice gauge theories [22]. Fracton phases are then constructed through a process of gauging the subsystem symmetries [51]. Another method to obtain fracton phases is by twisting the usual fracton models [52].

In this work, we present some novel models of fracton order based on lattice gauge theories in  $d = 2$  and  $d = 3$  spatial dimensions. While the 2-dimensional model is a known regular fracton model [48], the 3-dimensional one exhibits some features that are not present in any of the standard concrete realizations of fracton phases. The ground state degeneracy of this new model grows exponentially with the square of the linear size of the system, and there is also a topological contribution to the ground state degeneracy when the system is defined on topologically non-trivial manifolds. Moreover, while this new model has completely immobile fractons as some of its excitations, there are also quasi-particles in the spectrum that are fully mobile, going beyond the type-I and type-II classification for fracton phases. Even though some known models also present mobile charges [53], the method introduced here gives an alternative way of constructing fracton models that differs from the usual one based on generalized lattice gauge theory with subsystem symmetries. We also present a general way to construct models for fracton order in  $d = 2$  and  $d = 3$  dimensions from lattice gauge theories with arbitrary, possibly non-Abelian gauge groups, of which the previously mentioned new fracton models are special cases. We show some examples of fracton order arising from  $\mathbb{Z}_3$  lattice gauge theory and  $S_3$  lattice gauge theory. These new non-Abelian models host non-Abelian fractons at the same time that they host non-Abelian anyons, allowing the study of the interplay between those two types of exotic quasi-particles.

The outline of this paper is the following: in Section II, we introduce a 2-dimensional fracton model and describe its fracton properties. In Section III, we introduce the new 3-dimensional fracton model and analyze its fracton

properties, borrowing results obtained in Section II. In Section IV, we introduce the generalized models of fracton phases based on gauge theories with arbitrary finite gauge groups. We show, as examples, models based on  $\mathbb{Z}_3$  and  $S_3$  lattice gauge theory and calculate some of their fracton properties.

## II. REVIEW OF FRACTON ORDER IN TWO DIMENSIONS

In this section, we start by reviewing a simple example of a model exhibiting fracton order in two spatial dimensions. The  $2d$  model was first introduced in [54, 55] to describe a superconducting state and it is known as the Xu-Moore model or *plaquette Ising model*. The model is shown to have  $1d$  subsystem symmetry [51, 56] and thus considered as a model for fracton order [48] as we will see. Its classical version is known as the *gonihedric Ising model*, a particular case of the eight-vertex model [57], studied in the context of string theory and spin-glass physics in [58–61] and references therein. Although our  $3d$  model is not a generalization of this  $2d$  model, some of the computation turns out to be quite similar.

### A. The model

Consider the discretization of a 2-dimensional oriented manifold  $M$ . For simplicity, we take the discretization to be described by a square lattice  $K$ . The lattice is composed by a set of vertices  $K_0$ , a set of links  $K_1$  and plaquettes  $K_2$ . To each vertex  $v \in K_0$  we associate a local Hilbert space  $\mathcal{H}_v$  with basis  $\{|1\rangle, |-1\rangle\}$ . In other words a spin-1/2 degree of freedom sits at each vertex  $v$ . Consequently, the total Hilbert space of the model,  $\mathcal{H}$ , is given by the tensor product of the local Hilbert spaces over all vertices,

$$\mathcal{H} := \bigotimes_v \mathcal{H}_v. \quad (1)$$

For each plaquette  $p \in K_2$ , we define the operator

$$B_p = \frac{1}{2} \left( \bigotimes_{v \in p} \mathbb{1}_v + \bigotimes_{v \in p} \sigma_v^z \right), \quad (2)$$

that acts over the spins at the four vertices of  $p$ . This operator collects the values of spins at the vertices of  $p$ , such that it favors configurations with even number of  $|-1\rangle$  around plaquettes. Although this operator seems to be just comparing the degrees of freedom at the vertices around plaquettes, a more physical interpretation of its action will be given in section IV. The global  $\mathbb{Z}_2$  symmetry of the model is made part of the Hamiltonian by means of the projector

$$A = \frac{1}{2} \left( \bigotimes_{v \in K_0} \mathbb{1}_v + \bigotimes_{v \in K_0} \sigma_v^x \right), \quad (3)$$

where the tensor product is taken over all vertices in  $K_0$ . This operator enforces a global gauge transformation on the system. Given (2) and (3), the Hamiltonian is defined by:

$$H = -A - \sum_p B_p. \quad (4)$$

The global  $\mathbb{Z}_2$  operator  $X$  given by

$$X = \bigotimes_{v \in K_0} \sigma_v^x \quad (5)$$

commutes with  $H$ .

## B. Fracton properties

There seems to be two essential features that characterize fracton phases of matter: the subextensive behavior of the ground state degeneracy and the mobility constraints of the quasi-particles that belong to the spectrum of the model. The quasi-particles that are usually called fractons are completely immobile if considered individually. Bound states of fractons, however, can have increased mobility. The mobility constraints are also captured by more general descriptions such as the rank-2  $U(1)$  gauge theory [38] and the foliated field theory [50]. Here we show that the model defined in section II A has all the characteristics of a fracton phase.

### 1. Ground State Degeneracy

Since the operators  $A$  and  $B_p$  commute for every plaquette  $p$ , we can solve this Hamiltonian exactly. Moreover, the operators  $A$  and  $B_p$  are projectors, so their spectrum is known. This allows us to characterize the ground state subspace of the model as:

$$\mathcal{H}_0 = \{|\psi\rangle \in \mathcal{H} \mid A|\psi\rangle = |\psi\rangle \text{ and } B_p|\psi\rangle = |\psi\rangle\},$$

for every plaquette  $p \in K_2$ . Let us now construct such states. To start, let  $|+\rangle \in \mathcal{H}$  be the state where every vertex spin in the lattice is in the  $|+1\rangle_v$  configuration, namely

$$|+\rangle = \bigotimes_v |+1\rangle_v.$$

Similarly, the state where all local degrees of freedom are in the  $| -1\rangle_v$  state is written

$$|-\rangle = \bigotimes_v |-1\rangle_v.$$

It is not difficult to see that the two states above satisfy the condition  $B_p|\psi\rangle = |\psi\rangle$  for all plaquettes  $p \in K_2$ . Then, the state  $|\psi_0\rangle = A|+\rangle = A|-\rangle = \frac{1}{2}(|+\rangle + |-\rangle)$  is a ground state.

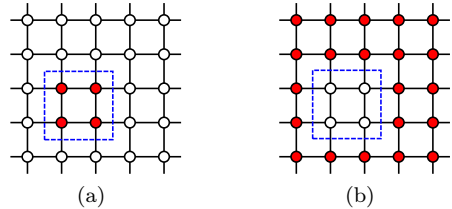


Figure 1. The domain wall (in blue) of (a) separates two regions with different spin configurations. The same domain wall also determines the separation between configurations of (b). More importantly, the configuration in (a) is gauge equivalent to that of (b).

Now, in order to construct other ground states, we will introduce a graphical notation to represent the basis states of  $\mathcal{H}$  as follows; one can color (red) any vertex that holds a  $| -1\rangle_v$  local degree of freedom, see figure 1. Furthermore, domain walls separating two regions with different spin configuration can be drawn. In general, a single domain wall is associated with two basis states of  $\mathcal{H}$ , as shown in figure 1. However, because of the global gauge transformation the two basis states associated to one domain wall diagram are gauge equivalent. This means that domain walls are enough to represent gauge equivalence classes of basis states, or *physical states*. For example, in figure 2 we show two domain wall diagrams and the respective states they represent.

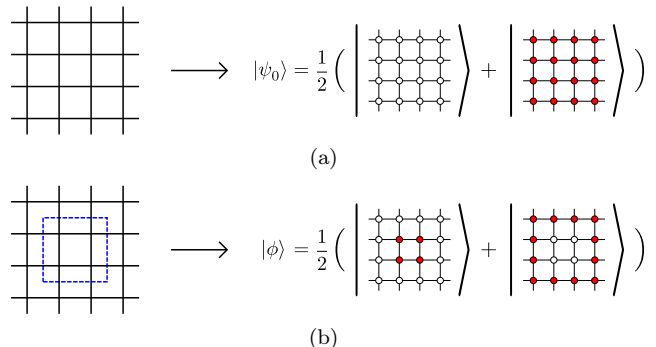


Figure 2. In (a) the domain wall diagram at the left represents the linear combinations of states at the right, in this case the ground state  $|\psi_0\rangle = A|+\rangle$ . In (b) the diagram at the left represents the state  $|\phi\rangle$ , which in fact is an excited state of the model.

The trivial ground state,  $|\psi_0\rangle$  is represented by a diagram with no domain walls, as shown in figure 2(a). On the other hand, the diagram at the left of figure 2(b) stands for a state resulting from a linear combination of states with the given domain wall configuration, this state is actually an elementary excited state of the model as we will see in section II B 2.

Other ground states are given by gauge-equivalence classes of states in  $\mathcal{H}$  on which  $B_p$  acts trivially (i.e., as an identity operator), for every  $p \in K_2$ . This means that every state obtained by applying the global gauge

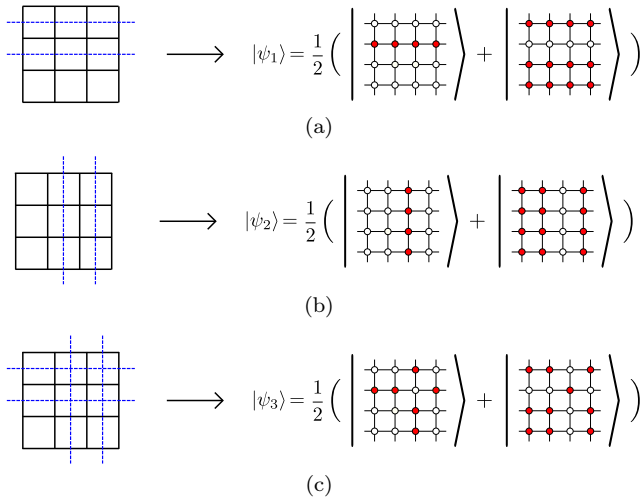


Figure 3. Some possible ground states of the model. The domain wall lines must begin and end at the boundary of the lattice.

transformation on a trivial eigenstate of  $B_p$ , for all  $p$ , is a ground state. In order to be invariant under  $B_p$ , a state must have either an even number of vertices with  $|-1\rangle_v$  spins at each plaquette of the lattice, or no  $|-1\rangle_v$  spins at all. The latter case is taken care of by the state  $|\psi_0\rangle$ . The former case is illustrated in figure 3. The domain wall lines must begin and end at the boundary of  $M$ . In case  $M$  has no boundary, the starting points of the blue domain wall lines must be identified with its ending points. Essentially, domain wall lines cannot have corners, i.e., every domain wall line that enters a plaquette must exit it in the diametrically opposite side, as opposed to figure 2(b), which clearly represents an excited state because it has plaquettes with an odd number of vertices with spin  $|-1\rangle$ . Since the global gauge transformation  $A$  does not change domain wall diagrams, any domain wall configuration that represents a (gauge equivalent) linear combination of trivial eigenstates of  $B_p$ , for every  $p$ , is a ground state.

Note that we can have ground states with an arbitrary number of domain wall lines in both directions. If the manifold has dimension  $L_x \times L_y$ , this means that we can construct  $2^{L_x}$  states with domain wall lines in the  $x$ -direction and  $2^{L_y}$  states with domain wall lines in the  $y$ -direction. The state with all horizontal lines is equivalent to the state with all vertical lines so discount this factor which yields a total of

$$GSD = 2^{L_x + L_y - 1} \quad (6)$$

possible ground states. This shows the sub extensive behavior of the ground state degeneracy, which is characteristic of fracton models. Equation (6) will be important when we consider the ground state of the  $3d$  model to be introduced in the next section.

## 2. Fracton excitations

The excited states of the model  $|\phi\rangle \in \mathcal{H}$  are states for which either  $A|\phi\rangle = 0$  or, for some plaquette  $p \in K_2$ ,  $B_p|\phi\rangle = 0$ . The excited state coming from the condition on the  $A$  operator is usually called *charge*. It is created by acting locally with  $\sigma^z$  on a single (arbitrary) vertex over a ground state of the model. The global nature of the gauge transformation makes it impossible to localize the charge, since we can only know whether a charge is present or not. For this reason, the charge is said to be global.

Plaquette excitations live at plaquettes that have a spin configuration with an odd number of vertices with spin  $|-1\rangle_v$ . Therefore, they live at the corners of domain walls. For example, the configuration in figure 2(b) has four excitations living at the four corners of the domain wall, as explicitly shown in figure 4. We can move pairs of excitations along straight lines, but individual excitations cannot be moved without costing energy to the system, and so they are essentially immobile. Therefore, plaquette excitations in this model are completely immobile fractons, and indeed the system described by the Hamiltonian in equation (4) exhibits fracton order in two dimensions. The arguments made for the calculation of the fracton properties of this model will be important to the study of other models we will define in the following sections.

## III. FRACTON ORDER IN THREE DIMENSIONS

Here we introduce a new model of fracton order in three spatial dimensions that exhibits some novel features, usually not present in the standard examples of fracton phases found in the literature. It is based on a  $\mathbb{Z}_2$  lattice gauge theory with slightly modified holonomy operators, as we show in the following subsection.

### A. The model

Let's consider a 3-dimensional manifold  $M$  discretized by a regular cubic lattice. At each link  $l$ , we have a spin-1/2 degree of freedom, and the total Hilbert space of the model, which we call  $\mathcal{H}$ , is a product of all Hilbert spaces that sit at every link of the lattice. For each vertex  $v$ , we define the local gauge transformation which acts over spins at each link that shares the vertex  $v$  as follows:

$$A_v \left| \begin{array}{c} \uparrow d \\ \leftarrow e \quad \rightarrow c \\ \downarrow b \quad \nearrow f \end{array} \right\rangle = \frac{1}{2} \left( \left| \begin{array}{c} \uparrow d \\ \leftarrow e \quad \rightarrow c \\ \downarrow b \quad \nearrow f \end{array} \right\rangle + \left| \begin{array}{c} \uparrow -d \\ \leftarrow -e \quad \rightarrow -c \\ \downarrow -b \quad \nearrow -f \end{array} \right\rangle \right), \quad (7)$$

where  $a, b, c, d, e, f \in \{1, -1\}$ .

Next, for each elementary cube  $c$ , we define three holonomy operators,  $B_c^{(x)}$ ,  $B_c^{(y)}$  and  $B_c^{(z)}$ . To write them

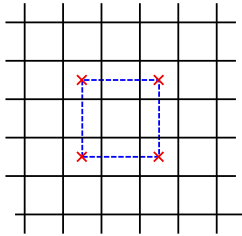


Figure 4. The configuration of figure 2(b) has four fractons, represented here as four red crosses.

in a neat way, we represent the action of  $\sigma^z$  operators by coloring links, that is, links in blue are the ones over which a  $\sigma^z$  operator act.

$$B_c^{(x)} \left| \begin{array}{c} \uparrow \\ \text{cube} \\ \downarrow \\ \leftarrow \text{ } \rightarrow \end{array} \right\rangle = \frac{1}{2} \left( \left| \begin{array}{c} \uparrow \\ \text{cube} \\ \downarrow \\ \leftarrow \text{ } \rightarrow \end{array} \right\rangle + \left| \begin{array}{c} \uparrow \\ \text{cube} \\ \downarrow \\ \leftarrow \text{ } \rightarrow \end{array} \right\rangle \right), \quad (8)$$

$$B_c^{(y)} \left| \begin{array}{c} \uparrow \\ \text{cube} \\ \downarrow \\ \leftarrow \text{ } \rightarrow \end{array} \right\rangle = \frac{1}{2} \left( \left| \begin{array}{c} \uparrow \\ \text{cube} \\ \downarrow \\ \leftarrow \text{ } \rightarrow \end{array} \right\rangle + \left| \begin{array}{c} \uparrow \\ \text{cube} \\ \downarrow \\ \leftarrow \text{ } \rightarrow \end{array} \right\rangle \right), \quad (9)$$

$$B_c^{(z)} \left| \begin{array}{c} \uparrow \\ \text{cube} \\ \downarrow \\ \leftarrow \text{ } \rightarrow \end{array} \right\rangle = \frac{1}{2} \left( \left| \begin{array}{c} \uparrow \\ \text{cube} \\ \downarrow \\ \leftarrow \text{ } \rightarrow \end{array} \right\rangle + \left| \begin{array}{c} \uparrow \\ \text{cube} \\ \downarrow \\ \leftarrow \text{ } \rightarrow \end{array} \right\rangle \right). \quad (10)$$

The operator  $B_c^{(\mu)}$ , for each direction  $\mu = x, y, z$ , checks if the holonomies of two opposite plaquettes in the direction  $\mu$  are equal. This is obtained by taking the product of holonomies of the two plaquettes in the boundary of  $c$  whose surfaces are orthogonal to  $\mu$ . If both plaquettes have the same holonomy, this product is equal to  $+1$  and we have an eigenstate of  $B_c^{(\mu)}$  with eigenvalue  $+1$ . Likewise, if the two opposing plaquettes have different holonomies, the product is equal to  $-1$  and we have an eigenstate of  $B_c^{(\mu)}$  with zero eigenvalue, an excited state. We will say that a state has trivial holonomy in the direction  $\mu$  if it is invariant under  $B_c^{(\mu)}$ , for every cube  $c$  in the lattice. The Hamiltonian is then given by

$$H = - \sum_v A_v - \sum_c \left( B_c^{(x)} + B_c^{(y)} + B_c^{(z)} \right). \quad (11)$$

## B. Fracton properties

### 1. Ground State Degeneracy

As in the 2D model, the operators  $A_v$  and  $B_c^{(\mu)}$  commute for all vertices  $v$ , cubes  $c$  and directions  $\mu$  in the lattice, so they can be diagonalized simultaneously. Also, the operators defined in equations (7), (8), (9) and (10) are all projectors. This implies that the ground state of the model is given by all gauge-equivalence classes of states with trivial holonomy in all directions. Therefore, we must search for states such that, at each cube of the lattice, opposite plaquettes at each direction have the same holonomy. A natural ground state is  $|\psi_0\rangle = \prod_v A_v |+\rangle$ , where  $|+\rangle \in \mathcal{H}$  is the state of the system where every link is in the  $|+1\rangle_l$  state. To visualize these states, we introduce a graphical notation as follows: whenever a link has spin  $|-1\rangle_l$ , we draw a blue dual plaquette, as shown in figure 5, while links with spin  $|+1\rangle_l$  have no additional drawings.

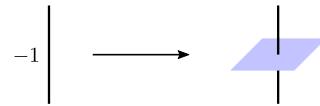


Figure 5. Links holding a  $|-1\rangle_l$  spin are represented by being crossed by a blue dual surface.

In this graphical notation, the action of  $A_v$ , for some vertex  $v$ , over the state  $|+\rangle$  is understood as introducing a blue closed surface around the vertex  $v$ . That is,

$$A_v \left| \begin{array}{c} \text{cube} \\ \text{cube} \\ \text{cube} \\ \text{cube} \end{array} \right\rangle = \frac{1}{2} \left( \left| \begin{array}{c} \text{cube} \\ \text{cube} \\ \text{cube} \\ \text{cube} \end{array} \right\rangle + \left| \begin{array}{c} \text{cube} \\ \text{cube} \\ \text{cube} \\ \text{cube} \end{array} \right\rangle \right), \quad (12)$$

where the vertex  $v$  is the one at the center of the cubic lattice. Therefore, the state  $|\psi_0\rangle$  is the superposition of all closed surfaces one can draw around vertices in the lattice and this ground state, as shown in equation (13), can be interpreted as a membrane gas much like the loop gas ground state of the toric code.

In the case that the manifold  $M$  has the topology of a 3-torus, non-contractible closed surfaces give different equivalence classes of ground states. This increases the *GSD* with topological terms. In other words, the ground states of the 3D toric code are also ground states of our model, and there is a purely topological contribution to the ground state of the Hamiltonian (11).

$$|\psi_0\rangle = N \left( \left| \begin{array}{c} \text{3D grid} \\ \text{no membrane} \end{array} \right\rangle + \left| \begin{array}{c} \text{3D grid} \\ \text{membrane at } x=1 \end{array} \right\rangle + \left| \begin{array}{c} \text{3D grid} \\ \text{membrane at } x=2 \end{array} \right\rangle + \left| \begin{array}{c} \text{3D grid} \\ \text{membrane at } x=3 \end{array} \right\rangle + \dots \right), \quad (13)$$

However, we are more interested in the contribution to the ground state of  $H$  that grows exponentially with the system size, the *subextensive terms*. For this reason we consider  $M$  as having the topology of a 3-dimensional ball with dimensions  $L_x \times L_y \times L_z$ . States represented by membranes beginning at one of the boundaries of  $M$  and ending at the diametrically opposite boundary are also ground states of the model. For instance, the state represented by figure 6(a). Membranes can have arbitrary shapes in every one of the three directions as long as they end at the boundaries of  $M$ , as in figure 6(b). If the membranes do not end at the boundaries of  $M$ , we have an excited state, as in figure 8(a), where we have a link with spin  $|-1\rangle$  shared by four cubes, which yields an excited state of cube operators in the  $z$  and  $y$  directions. In the interior of  $M$ , membranes cannot bend to perpendicular directions, for if they do we get excitations of cube operators at the folding regions of the bent membranes, as in figure 8(b) where the membrane of figure 8(a) is folded into the  $x$  direction, giving rise to excitations of  $B_c^{(x)}$  operators at the folding line. The gauge transformation acts at vertices and can be pictured as adding a closed (dual) surface around the vertex it acts, see eq. (12). Thus, gauge transformations can only deform membranes without changing their boundary.

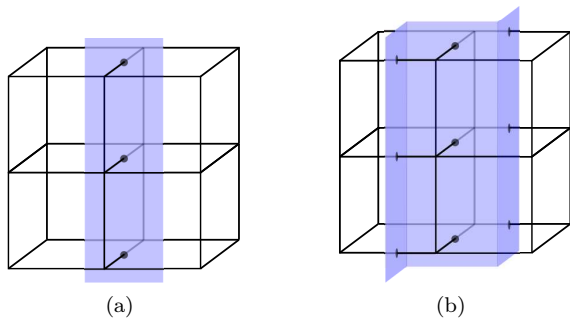


Figure 6. We show two possible ground state configurations of Hamiltonian in (11). The membrane must begin at the boundary of  $M$  and end at the diametrically opposite region. This means that, inside  $M$ , the membrane cannot curve to perpendicular directions.

We can have arbitrary compositions of such membrane configurations in every direction. Since the boundary lines of the membranes are gauge-invariant, we use them to count how many possible ground state configurations we can construct in this model. Note that if we project figure 6(a) into a plane and only draw the boundary lines of the membrane, as in figure 7, we get exactly the same

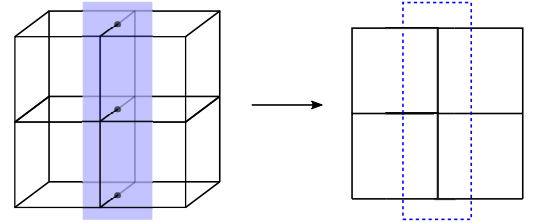


Figure 7. Figure 6(a) projected along the  $x$ -axis. We remove the coloring showing the membrane itself and instead focus on the boundary. Note that this corresponds exactly to the domain wall notation of section II.

graphical picture for the ground states we had in the 2D model of section II. This means that we essentially have stacks of the ground states of the 2D model in all directions. Since  $M$  has dimensions  $L_x \times L_y \times L_z$ , we can draw  $(2^{L_y+L_z-1})^{L_x}$  states in the  $L_x$  direction,  $(2^{L_x+L_z-1})^{L_y}$  states in the  $L_y$  direction and  $(2^{L_x+L_y-1})^{L_z}$  in the  $L_z$  direction, giving a total of

$$GSD = 2^{2(L_x L_y + L_x L_z + L_y L_z) - L_x - L_y - L_z} \quad (14)$$

possible ground states. It is useful to think of the ground states of this model as condensations of the the 3D Toric Code model. Note that every ground state of the 3D Toric Code is a ground state of our model. Moreover, some excited states of the 3D Toric Code are ground states of our model. In particular, the flux excitations of the TC that lie on a single plane are ground states of our model as well.

## 2. Fracton excitations

The elementary excited states  $|\phi\rangle \in \mathcal{H}$  are such that either  $A_v |\phi\rangle = 0$ , for some vertex  $v$ , or  $B_c^{(\mu)} |\phi\rangle = 0$ , for some cube  $c$  and direction  $\mu$ . A string of  $\sigma^z$  operators, beginning at a vertex  $v$  and ending at a vertex  $v'$ , creates excitations of  $A_v$  and  $A_{v'}$ , also called charge excitations. Since  $A_v$  is essentially the gauge transformation of the 3D toric code, the charge excitations of the model (11) are the same charge excitations of the 3D Toric Code, and they can move freely in the lattice without an energy cost.

Now, excited states of the cube operators  $B_c^{(\mu)}$  are called  $\mu$ -flux excitations and can be pictured as lying at the corners of membranes. This can be better understood using the graphical representation of states as in figure 8. The simplest  $\mu$ -flux excited state is created by

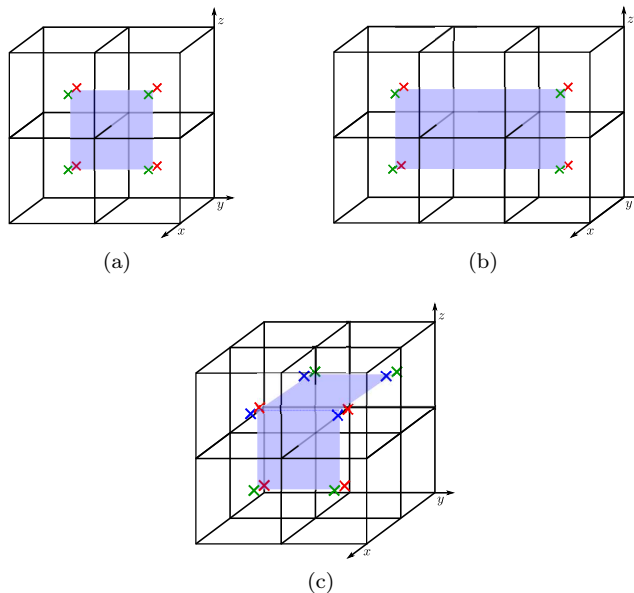


Figure 8. (a) An state represented by the membrane diagram inside  $M$  has flux excitations and the four cubes at its corners. The red crosses represent what we call  $z$ -fluxes, excitations of  $B_c^{(z)}$ . Whereas the green ones are  $y$ -fluxes, excitations of  $B_c^{(y)}$ . Blue crosses stand for  $x$ -fluxes, excitations of  $B_c^{(x)}$  (b) Excitations can freely move as long as the number of corners remains invariant. (c) If a membrane bends into a orthogonal direction, flux excitations are created at every corner it has.

the action of a  $\sigma^x$  operator on a single site over a ground state of the model. Note that whether this operator acts on a link along the  $x, y$  or  $z$ -axis will result on certain combinations of  $x, y$  and  $z$ -fluxes. For instance, acting with  $\sigma_l^x$  on a ground state:

$$|\phi\rangle = \sigma_l^x |\psi_0\rangle, \quad (15)$$

where  $l$  is a  $x$ -like link, results on a state with pairs of  $y$  and  $z$ -fluxes at the boundaries of the membrane as depicted in figure 8(a).

These excitations have restricted mobility since their localization is associated to the corners of the membrane. For example, the state represented by figure 8(b) shows that extending the membrane along the  $y$ -direction move pairs of  $\mu$ -fluxes. In general, moving these excitations correspond to extending the membrane without changing the number of corners. On the contrary, if the membrane is bent towards its orthogonal direction more excited states are created increasing the energy of the state, as shown in figure 8(c). Again, this is interpreted as an energy penalization to deformations of membranes that change their number of corners.

### 3. Relaxing Mobility Restrictions

The  $\mu$ -fluxes of the Hamiltonian (11) are only able to move without energy cost along planes. Take for instance the excited state represented in figure 8(a) with four pairs of  $(y, z)$ -fluxes, one at each corner of the membrane. The pairs of fluxes at corners are free to move in the  $(y, z)$

plane by deforming the membrane as long as the number of corners remains invariant. However, if the membrane is to be bent into any of the two orthogonal directions the resulting state's energy increases. This is understood as an *energy penalization* to the bending of membranes, see figure 8(b). The membranes get these mobility restrictions from the holonomy terms in equation (11) or  $B_c^{(\mu)}$  operators for  $\mu = \{x, y, z\}$ . In particular, the operator  $B_c^{(x)}$  penalizes configurations where a membrane enters the cube  $c$  in the  $x$  direction and leaves the cube heading either the  $y$  or  $z$  direction.

Since each holonomy term of equation (11) is responsible for penalizing the bending of a membrane at a certain direction, mobility restrictions of  $\mu$ -fluxes can be partially lifted by taking  $B_c^{(\mu)}$  operators and replacing them with plaquette operators acting over plaquettes orthogonal to the  $\mu$  direction. To see that this is true, we consider Hamiltonians slightly different to that of (11), namely,

$$H_{(\mu, \nu)} = - \sum_v A_v - \sum_c \left( B_c^{(\mu)} + B_c^{(\nu)} \right) - \sum_{\substack{p \perp \tau \\ \tau \neq \mu, \nu}} B_p, \quad (16)$$

$$H_{(\mu)} = - \sum_v A_v - \sum_c B_c^{(\mu)} - \sum_{\substack{p \perp \nu \\ \nu \neq \mu, \tau}} B_p - \sum_{\substack{p \perp \tau \\ \tau \neq \mu, \nu}} B_p, \quad (17)$$

where  $\mu, \nu, \tau = \{x, y, z\}$  and the new terms added to the Hamiltonian are usual plaquette operators of the toric code acting over plaquettes that are perpendicular to certain directions. To illustrate, consider the Hamiltonian

$H_{(x,y)}$ . The comparison between 1-holonomies of plaquettes in the  $x$  and  $y$  directions is still present in the form of the term  $\sum_c (B_c^{(x)} + B_c^{(y)})$  as in (11), but now there is a term  $\sum_{p \perp z} B_p$  that only measures the 1-holonomies of plaquettes perpendicular to the  $z$  direction. The fracton fluxes are still created at the corner of membranes. However, the quasi-particles at the corners of every membrane that is perpendicular to the  $xy$  plane are now regular flux excitations of the toric code, i.e., they are free to move along planes parallel to the  $xy$  plane. In this way we can think of our general model (11) as describing a condensation of flux excitations of the toric code in every spatial direction, while the models in equations (16) and (17) describe condensations of toric code fluxes in some particularly chosen directions.

#### IV. GENERALIZATIONS TO ARBITRARY GAUGE GROUPS

The models presented in sections II and III are special cases of a more general class of models based on arbitrary, possibly non-Abelian finite groups. In this section, we introduce such general models and show some examples for groups other than  $\mathbb{Z}_2$ . That is, instead of considering as degrees of freedom elements of  $\mathbb{Z}_2$ , as we did in the previous sections, we will take them as elements of some arbitrary finite group  $G$ .

##### A. $G$ -Fracton order in two dimensions

Consider a 2-dimensional oriented manifold  $M$ , discretized by a square lattice. At each vertex  $v$ , we have a local Hilbert space  $\mathcal{H}_v$  with basis given by states  $|g\rangle$  labelled by some element  $g \in G$ , where  $G$  is an arbitrary finite group and the total Hilbert space is  $\mathcal{H} = \bigotimes_v \mathcal{H}_v$ . Global gauge transformations are given by

$$A^g |a, b, c, \dots\rangle = |ag, bg, cg, \dots\rangle, \quad (18)$$

where  $g \in G$  and  $|a, b, c, \dots\rangle \in \mathcal{H}$  is an arbitrary basis state in the total Hilbert space, with  $a, b, c, \dots \in G$ . We define the operator  $A$  as the normalized sum of all global gauge transformations, namely,

$$A = \frac{1}{|G|} \sum_{g \in G} A^g. \quad (19)$$

One can easily see that if  $G = \mathbb{Z}_2$ , we recover equation (3). Next, we define two plaquette operators  $B_p^{(\mu)}$ ,  $\mu = x, y$ , which in the language of higher gauge theories (see [20]), act by comparing the 0-holonomy of links that are parallel to the  $\mu$  direction. They are given by the

formulas

$$B_p^{(x)} \left| \begin{array}{cc} d & c \\ \uparrow & \uparrow \\ a & b \end{array} \right\rangle = \delta(ab^{-1}, dc^{-1}) \left| \begin{array}{cc} d & c \\ \uparrow & \uparrow \\ a & b \end{array} \right\rangle, \quad (20)$$

$$B_p^{(y)} \left| \begin{array}{cc} d & c \\ \uparrow & \uparrow \\ a & b \end{array} \right\rangle = \delta(ad^{-1}, bc^{-1}) \left| \begin{array}{cc} d & c \\ \uparrow & \uparrow \\ a & b \end{array} \right\rangle. \quad (21)$$

If  $G$  is Abelian, the two operators are actually the same, and one can easily check that if  $G = \mathbb{Z}_2$ , we recover equation (2). The Hamiltonian is then given by

$$H = -A - \sum_p (B_p^{(x)} + B_p^{(y)}). \quad (22)$$

From here on, we can work out some specific examples of this model where the gauge group is other than  $\mathbb{Z}_2$ .

##### 1. 2D Examples

###### $\mathbb{Z}_3$ -Fracton Order in 2D:

Let  $G = \mathbb{Z}_3$ , where  $\mathbb{Z}_3$  is the cyclic group given by  $\mathbb{Z}_3 = \{1, \omega, \omega^2\}$ , where  $\omega = e^{2\pi i/3}$ . Since  $\mathbb{Z}_3$  is Abelian,  $B_p^{(x)} = B_p^{(y)} = B_p$ , for every plaquette  $p$  in the lattice, and it is given by

$$B_p \left| \begin{array}{cc} d & c \\ \uparrow & \uparrow \\ a & b \end{array} \right\rangle = \delta(ab^{-1}, dc^{-1}) \left| \begin{array}{cc} d & c \\ \uparrow & \uparrow \\ a & b \end{array} \right\rangle. \quad (23)$$

The operator  $A$  of equation (19) is given by

$$A = \frac{1}{3} (A^1 + A^\omega + A^{\omega^2}), \quad (24)$$

where each  $A^g, g \in \mathbb{Z}_3$ , acts over basis states as in equation (18) by multiplying every degree of freedom by  $g$ .

The ground states of the Hamiltonian (22) can be built from eigenstates of  $B_p$  with eigenvalue 1, for every  $p$ . This is better seen using a domain wall representation of physical states similar to the one introduced in section II. The difference being that domain walls separating  $\omega$  and  $\omega^2$  degrees of freedom have to be distinguished. We do that by giving an orientation to the domain wall lines in the following way: a domain wall surrounding a  $\omega$  configuration is oriented clockwise, while a domain wall surrounding a  $\omega^2$  configuration is oriented counter-clockwise, as in figure 9. This notation allows to count the number of independent ground states, as in section II. We just need to count all combinations of domain walls with straight lines as boundaries similar to the ones in



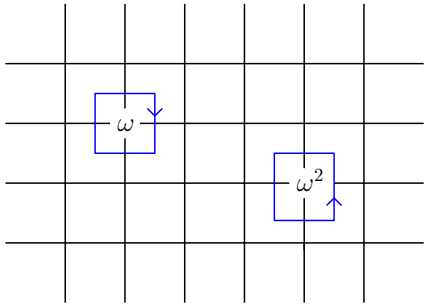


Figure 9. Domain wall notation for the  $\mathbb{Z}_3$ -spins.

figure 3. Here we have oriented domain walls which increases the number of possible configurations. In particular, it is not hard to check that if  $M$  is a manifold with boundaries of dimension  $L_x \times L_y$ , there are

$$GSD_{2D, \mathbb{Z}_3} = 3^{L_x + L_y - 2} \quad (25)$$

possible ground states.

Plaquette excitations of this model are also fractons living at the corners of domain walls. Despite the fact that there are two kinds of domain walls in our notation, all fractons are of the same nature, for the plaquette operator cannot distinguish to which type of domain wall the fracton it detects is associated.

#### $S_3$ -Fracton Order in 2D:

Now, let  $G = S_3$ , the group of all permutations of three objects, given by  $S_3 = \{e, \alpha, \alpha^2, \beta, \beta\alpha, \beta\alpha^2\}$ , with relations  $\alpha^3 = \beta^2 = e$ ,  $\beta\alpha = \alpha^2\beta$  and so on.  $S_3$  is non-Abelian, so we have both operators  $B_p^{(x)}$  and  $B_p^{(y)}$ , for every plaquette  $p$ , as given in equations (20) and (21). The operator  $A$  of equation (19) is given by

$$A = \frac{1}{6} \left( A^e + A^\alpha + A^{\alpha^2} + A^\beta + A^{\beta\alpha} + A^{\beta\alpha^2} \right). \quad (26)$$

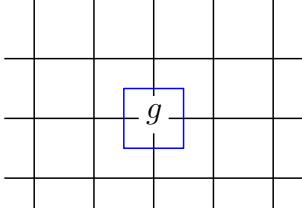
Ground states of the Hamiltonian (22) for this model can be obtained from eigenstates with eigenvalue 1 of both  $B_p^{(x)}$  and  $B_p^{(y)}$  simultaneously. As in the Abelian case, we can use a graphical notation to represent the states: around a vertex with a degree of freedom labelled

by  $g \in S_3$ , we draw a domain wall labelled by  $g$ , as in figure 10. We have to be careful about the order in which we superpose domain wall figures, for the elements of the group do not commute. Ground state configurations are thus those in which we have straight lines, with a given label, connecting diametrically opposite boundary points in the two directions. We can have alternating lines of different labels, but the only two non-trivial different lines that can intercept each other at a given point are the ones labelled by  $\alpha$  and  $\alpha^2$ . From those considerations, the ground state degeneracy can be calculated by noticing that the subgroup of  $S_3$  given by  $\{e, \alpha, \alpha^2\}$  is isomorphic to  $\mathbb{Z}_3$ , while the subgroups  $\{e, \beta\}$ ,  $\{e, \beta\alpha\}$  and  $\{e, \beta\alpha^2\}$  are isomorphic to  $\mathbb{Z}_2$ . Consider domain wall lines labelled only by the subgroup  $\{e, \alpha, \alpha^2\}$ . This situation is equivalent to the  $\mathbb{Z}_3$ -fracton model studied before, and thus this choice of labels contributes with  $3^{L_x + L_y - 2}$  ground states. Next, consider domain wall lines labelled by the subgroups  $\{e, \beta\}$ ,  $\{e, \beta\alpha\}$  or  $\{e, \beta\alpha^2\}$ . Each of these subgroups correspond to a  $\mathbb{Z}_2$ -fracton model and thus there are  $3 \times 2^{L_x + L_y - 1}$  ground states coming from those subgroups. Last, we must consider the case where there are lines with labels coming from different subgroups. There are  $6^{L_x}$  possibilities of drawing such lines in the  $x$ -direction and  $6^{L_y}$  possibilities in the  $y$ -direction, but bear in mind that lines with labels coming from different subgroups cannot cross each other. Therefore, discounting how many extra times we have included lines labelled by the identity element of the group, the number of ground states is given by equation (27) and it also behaves sub extensively with the system's size. However, this behavior is not given by a simple formula as in the Abelian case, because only a limited number of lines can intercept each other. This can be interpreted by noting that a line that connects diametrically opposite boundary points may be represented as a sub-system symmetry operator, i.e., a symmetry operator that only acts over a sub-dimensional region of the lattice, that is, over a line or a set of lines. The sub-system symmetry operator associated to a ground state line is an operator that acts over the seed state by multiplying the  $S_3$ -spins along the line by some group element. The fact that two arbitrary intercepting lines does not give a ground state means that, due to the non-Abelian nature of  $S_3$ , arbitrary compositions of sub-system symmetry operators do not in general result in another sub-system symmetry operator.

$$GSD_{2D, S_3} = 3 \times 2^{L_x + L_y - 1} + 3^{L_x + L_y - 2} + 6^{L_x} + 6^{L_y} - 5, \quad (27)$$

The excitations of the  $A$  operator are global non-Abelian charges. The flux excitations of this model are also fractons, living at corners of domain walls, but now we can have two types of them:  $x$ -fluxes, excitations of

the operator  $B_p^{(x)}$ , and  $y$ -fluxes, excitations of the operator  $B_p^{(y)}$ . One can expect that, due to the non-Abelian nature of  $S_3$ , there will be complicated fusion and braiding rules for those quasi-particles, whose computation is

Figure 10. Domain wall notation for  $S_3$ -spins.

not within the scope of this present work.

### B. $G$ -Fracton order in three dimensions

Consider a 3-dimensional oriented manifold  $M$ , discretized by a regular cubic lattice. At each link  $l$ , there is a local Hilbert space  $\mathcal{H}_l$ , generated by a set  $\{|g\rangle\}$  of basis elements, labelled by some finite group  $G$ . The total

Hilbert space is given by the product  $\mathcal{H} = \bigotimes_l \mathcal{H}_l$ . For each vertex  $v$ , we define the local gauge transformation as

$$A_v = \frac{1}{|G|} \sum_{g \in G} A_v^g, \quad (28)$$

where  $A_v^g$ , for each  $g \in G$ , acts over basis states as follows:

$$A_v^g \left| \begin{array}{c} d \\ \swarrow e \quad \searrow c \\ \leftarrow a \quad \rightarrow b \quad \rightarrow f \end{array} \right\rangle = \left| \begin{array}{c} gd \\ \swarrow eg^{-1} \quad \searrow gc \\ \leftarrow ag^{-1} \quad \rightarrow bg^{-1} \quad \rightarrow gf \end{array} \right\rangle. \quad (29)$$

Next, we define three cube operators  $B_c^{(\mu)}$ , one for each direction  $\mu = x, y, z$ .  $B_c^{(\mu)}$  compares the 1-holonomy of plaquettes that are orthogonal to the  $\mu$  direction, in the following way:

$$B_c^{(x)} \left| \begin{array}{c} z \\ \swarrow b_4 \quad \searrow b_2 \\ \leftarrow b_1 \quad \rightarrow b_3 \\ \leftarrow a_4 \quad \rightarrow a_2 \\ \leftarrow a_1 \quad \rightarrow a_3 \\ \leftarrow c_4 \quad \rightarrow c_2 \\ \leftarrow c_1 \quad \rightarrow c_3 \end{array} \right\rangle = \delta(a_1 c_1 b_1^{-1} c_4^{-1}, a_3 c_2 b_3^{-1} c_3^{-1}) \left| \begin{array}{c} z \\ \swarrow b_4 \quad \searrow b_2 \\ \leftarrow b_1 \quad \rightarrow b_3 \\ \leftarrow a_4 \quad \rightarrow a_2 \\ \leftarrow a_1 \quad \rightarrow a_3 \\ \leftarrow c_4 \quad \rightarrow c_2 \\ \leftarrow c_1 \quad \rightarrow c_3 \end{array} \right\rangle, \quad (30)$$

$$B_c^{(y)} \left| \begin{array}{c} z \\ \swarrow b_4 \quad \searrow b_2 \\ \leftarrow b_1 \quad \rightarrow b_3 \\ \leftarrow a_4 \quad \rightarrow a_2 \\ \leftarrow a_1 \quad \rightarrow a_3 \\ \leftarrow c_4 \quad \rightarrow c_2 \\ \leftarrow c_1 \quad \rightarrow c_3 \end{array} \right\rangle = \delta(a_2 c_2 b_2^{-1} c_1^{-1}, a_4 c_4 b_4^{-1} c_4^{-1}) \left| \begin{array}{c} z \\ \swarrow b_4 \quad \searrow b_2 \\ \leftarrow b_1 \quad \rightarrow b_3 \\ \leftarrow a_4 \quad \rightarrow a_2 \\ \leftarrow a_1 \quad \rightarrow a_3 \\ \leftarrow c_4 \quad \rightarrow c_2 \\ \leftarrow c_1 \quad \rightarrow c_3 \end{array} \right\rangle, \quad (31)$$

$$B_c^{(z)} \left| \begin{array}{c} z \\ \swarrow b_4 \quad \searrow b_2 \\ \leftarrow b_1 \quad \rightarrow b_3 \\ \leftarrow a_4 \quad \rightarrow a_2 \\ \leftarrow a_1 \quad \rightarrow a_3 \\ \leftarrow c_4 \quad \rightarrow c_2 \\ \leftarrow c_1 \quad \rightarrow c_3 \end{array} \right\rangle = \delta(a_1 a_2 a_3^{-1} a_4^{-1}, b_1 b_2 b_3^{-1} b_4^{-1}) \left| \begin{array}{c} z \\ \swarrow b_4 \quad \searrow b_2 \\ \leftarrow b_1 \quad \rightarrow b_3 \\ \leftarrow a_4 \quad \rightarrow a_2 \\ \leftarrow a_1 \quad \rightarrow a_3 \\ \leftarrow c_4 \quad \rightarrow c_2 \\ \leftarrow c_1 \quad \rightarrow c_3 \end{array} \right\rangle. \quad (32)$$

We always have the three operators, even if  $G$  is Abelian, contrary to the two-dimensional case. Note that, if  $G = \mathbb{Z}_2$ , we recover equations (7), (8), (9) and (10). The Hamiltonian is defined as

$$H = - \sum_v A_v - \sum_c \left( B_c^{(x)} + B_c^{(y)} + B_c^{(z)} \right), \quad (33)$$

The operators defined in equation (29), (30), (31) and (32) commute for every vertex and cube in the lattice, so the Hamiltonian (33) can be diagonalized. Now we can produce some examples of models of fracton order for groups other than  $\mathbb{Z}_2$  and compute their fracton properties.

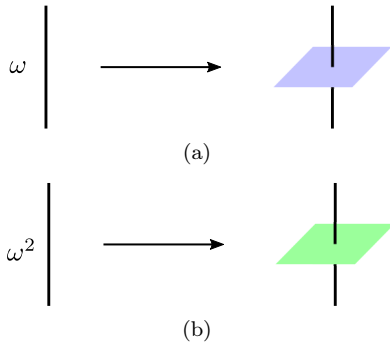
#### 1. 3D Examples

##### $\mathbb{Z}_3$ -Fracton Order in 3D:

First, let  $G = \mathbb{Z}_3$ , where  $\mathbb{Z}_3$  is given as in subsection IV A. The cube operators are as in eqns. (30), (31) and (32), while the gauge transformation at each vertex  $v$  is given by

$$A_v = \frac{1}{3} \left( A_v^1 + A_v^\omega + A_v^{\omega^2} \right), \quad (34)$$

where each  $A_v^g$ ,  $g \in \mathbb{Z}_3$ , acts as in eq. (29). The ground states of this model can be obtained from eigenstates with eigenvalue 1 of all cube operators simultaneously. We

Figure 11. Graphical language for the  $\mathbb{Z}_3$ -spins.

can use roughly the same graphical notation for states in this model as the one introduced in section III, but now we must distinguish between links carrying a  $\omega$  spin from links carrying a  $\omega^2$  spin, which is done in figure 11, where we associate a  $\omega$  spin at a link to a dual blue plaquette and a  $\omega^2$  spin at a link to a dual green plaquette. The ground states are then represented by the same type of surfaces of section III, the only difference being that here there are surfaces of two different colors, and the colors cannot mix, i.e., they cannot superpose each other, because the membrane vanishes in the region where there is a superposition of two colors, leaving a membrane with corners in the interior of the manifold, which corresponds to an excited state. The local gauge transformation only deforms colored membranes around a vertex without modifying its boundary lines, so the same counting argument based on the  $2D$  model used in section III also holds, and we have

$$GSD_{3D, \mathbb{Z}_3} = 3^{2(L_x L_y + L_x L_z + L_y L_z - L_x - L_y - L_z)} \quad (35)$$

ground states in a 3-manifold  $M$  with dimensions  $L_x \times L_y \times L_z$ .

In this model, the charge excitations, living on vertices of the lattice, are fully mobile, while the  $\mu$ -flux excitations, one for each  $\mu = x, y, z$ , are fractons living on

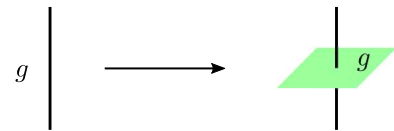
cubes, with the same properties as the ones in the  $\mathbb{Z}_2$  case.

### $S_3$ -Fracton Order in 3D:

Now, let  $G = S_3$ , where  $S_3$  is given as in subsection IV A. The cube operators are as in equations (30), (31) and (32) while the local gauge transformation, for each vertex  $v$ , is given by

$$A_v = \frac{1}{6} \left( A_v^e + A_v^\alpha + A_v^{\alpha^2} + A_v^\beta + A_v^{\beta\alpha} + A_v^{\beta\alpha^2} \right). \quad (36)$$

Ground states can be constructed from eigenstates with eigenvalue 1 of each one of the cube operators simultaneously. We can use the following graphical notation to represent the states: each link with some degree of freedom labelled by  $g \in G$  will be associated to a link crossing a dual plaquette labelled by  $g$ , as in figure 12. Since the group is non-Abelian, one must be careful with the order in which two dual plaquettes cross each other. Ground states are represented by surfaces of the type described in section III, but here there are some constraints to be obeyed. For example, the only two non-trivial different surfaces that can cross each other are the ones labelled by  $\alpha$  and  $\alpha^2$ , analogously to the  $2d$   $S_3$ -fracton model. The local gauge transformations act by adding labelled surfaces around vertices without altering the boundary lines of membranes, so ground states of this model can also be interpreted as a stack of layers of ground states of the  $2d$   $S_3$ -fracton model, and the ground state degeneracy can be calculated to be

Figure 12. Graphical language for the  $S_3$ -spins.

$$GSD_{3D, S_3} = (GSD_{2D, S_3})^{L_x} (GSD_{2D, S_3})^{L_y} (GSD_{2D, S_3})^{L_z}, \quad (37)$$

where  $GSD_{2D, S_3}$  is the ground state degeneracy of the 2-dimensional  $S_3$ -fracton of equation (27).

The charge excitations of this model are non-Abelian anyons living at vertices of the lattice. The  $\mu$ -flux excitations live at cubes and are non-Abelian fractons, with the same mobility restrictions as in the usual  $\mathbb{Z}_2$  case, but possibly with more complicated fusion and braiding rules, whose computation is not within the scope of this present work.

## V. CONCLUSIONS AND OUTLOOK

In this work, we have introduced new models of fracton order based on lattice gauge theory in two and three spatial dimensions. The 3-dimensional model exhibits some features that are usually not present in the most common realizations of fracton order, such as a ground state degeneracy that depends exponentially on square of the linear size of the system and on its topology, and fully

mobile excitations living along with fractons. These models show that one can obtain fracton phases from more regular lattice gauge theories, giving an alternative to the usual construction based on a gauging procedure of subsystem symmetries of generalized lattice gauge theories. We also introduced a way to construct 2 and 3-dimensional fracton models based on lattice gauge theories with arbitrary finite gauge groups. As examples, we constructed fracton models from  $\mathbb{Z}_3$  and  $S_3$  lattice gauge theory. These models also exhibit a ground state degeneracy that grows exponentially with the square of the linear size of the system and mobile anyons living along with fractons.

One important open question is how the models introduced in this work and more standard models such as the X-cube model are connected. Since the ground state degeneracy of the model described in section III scales differently from the X-cube, a relation between the two is not obvious. Also, the definitions of the models in sections II, III and IV show an explicit dependence on the geometry and the topology of the system, which suggests that new phenomena may arise if we define the models in manifolds with non-trivial geometry, topology and discretization. This direction was pursued for the X-cube model [62, 63], and therefore it may also be helpful in the

quest to clarify how the two models are connected. Furthermore, the possibility of constructing fracton models from non-Abelian gauge groups allows us to study more directly the behavior of non-Abelian fractons, which are known in the literature [52, 64], and its relation to non-Abelian anyons. This study could possibly lead to a better understanding on how to apply fracton phases in quantum computation. On the other hand, the entanglement entropy can certainly give more information about the nature of entanglement in the ground/excited states of the fracton models we introduce in this work. In [65], we show that the entanglement entropy calculation can be mapped into the counting of edge states in the entanglement cut. Whether this also holds for the fracton models of this work -or more general fracton models for that matter- is a question worthy of further study and that could deepen our understanding of gapped quantum phases of matter.

#### ACKNOWLEDGMENTS

JPIJ thanks CNPq (Grant No. 162774/2015-0) for support during this work. LNQX thanks CNPq (Grant No. 164523/2018-9) for supporting this work.

- 
- [1] D. C. Tsui, H. L. Stormer, and A. C. Gossard. *Phys. Rev. Lett.*, 48(22):1559, 1982.
  - [2] R. B. Laughlin. Anomalous Quantum Hall Effect: An Incompressible Quantum Fluid with Fractionally Charged Excitations. *Phys. Rev. Lett.*, 50:1395–1398, May 1983.
  - [3] X. G. Wen and Q. Niu. *Phys. Rev. B*, 41(13):9377, 1990.
  - [4] Xie Chen, Zheng-Cheng Gu, and Xiao-Gang Wen. *Phys. Rev. B*, 82(15):155138, 2010.
  - [5] A. Kitaev. *Ann. Phys.*, 303:2–30, 2003.
  - [6] Chetan Nayak, Steven H. Simon, Ady Stern, Michael Freedman, and Sankar Das Sarma. *Rev. Mod. Phys.*, 80(3):1083, 2008.
  - [7] Hector Bombin and M. A. Martin-Delgado. *Phys. Rev. B*, 78(11):115421, 2008.
  - [8] Oliver Buerschaper and Miguel Aguado. *Phys. Rev. B*, 80(15):155136, 2009.
  - [9] Miguel Jorge Bernabé Ferreira, Pramod Padmanabhan, and Paulo Teotonio-Sobrinho. *J. Phys. A: Math. Theor.*, 47(37):375204, 2014.
  - [10] Xie Chen, Zheng-Cheng Gu, Zheng-Xin Liu, and Xiao-Gang Wen. *Science*, 338(6114):1604–1606, 2012.
  - [11] Xie Chen, Zheng-Cheng Gu, Zheng-Xin Liu, and Xiao-Gang Wen. *Phys. Rev. B*, 87:155114, Apr 2013.
  - [12] Anton Kapustin. *arXiv preprint arXiv:1403.1467*, 2014.
  - [13] Vladimir G. Turaev and Alexis Virelizier. *Monoidal Categories and Topological Field Theory*, volume 322. Springer, 2017.
  - [14] Michael A. Levin and Xiao-Gang Wen. *Phys. Rev. B*, 71:045110, Jan 2005.
  - [15] John Baez and Urs Schreiber. *arXiv preprint math/0511710*, 2005.
  - [16] John Baez and John Huerta. *Gen. Rel. Grav.*, 43(9):2335–2392, 2011.
  - [17] Alex Bullivant, Marcos Calçada, Zoltán Kádár, Paul Martin, and Joao Faria Martins. *Phys. Rev. B*, 95(15):155118, 2017.
  - [18] Anton Kapustin and Ryan Thorngren. *arXiv preprint arXiv:1309.4721*, 2013.
  - [19] Clement Delcamp and Apoorv Tiwari. *J. High Energy Phys.*, 2018(10):49, 2018.
  - [20] R. Costa de Almeida, J. P. Ibieta-Jimenez, J. Lorca Espiro, and P. Teotonio-Sobrinho. *arXiv preprint arXiv:1711.04186*, 2017.
  - [21] Claudio Chamon. *Phys. Rev. Lett.*, 94(4):040402, 2005.
  - [22] Sagar Vijay, Jeongwan Haah, and Liang Fu. *Phys. Rev. B*, 94(23):235157, 2016.
  - [23] Rahul M. Nandkishore and Michael Hermele. *arXiv preprint arXiv:1803.11196*, 2018.
  - [24] Zack Weinstein, Emilio Cobanera, Gerardo Ortiz, and Zohar Nussinov. *arXiv preprint arXiv:1812.04561*, 2018.
  - [25] Jeongwan Haah. *Phys. Rev. A*, 83(4):042330, 2011.
  - [26] Claudio Castelnovo, Claudio Chamon, and David Sherrington. *Phys. Rev. B*, 81(18):184303, 2010.
  - [27] Claudio Castelnovo and Claudio Chamon. *Philosophical Magazine*, 92(1-3):304–323, 2012.
  - [28] Isaac H. Kim and Jeongwan Haah. *Phys. Rev. Lett.*, 116(2):027202, 2016.
  - [29] Abhinav Prem, Jeongwan Haah, and Rahul Nandkishore. *Phys. Rev. B*, 95(15):155133, 2017.
  - [30] Shriya Pai, Michael Pretko, and Rahul M Nandkishore. *Phys. Rev. X*, 9(2):021003, 2019.
  - [31] Sergey Bravyi and Jeongwan Haah. *Phys. Rev. Lett.*, 107(15):150504, 2011.

- [32] Sergey Bravyi, Bernhard Leemhuis, and Barbara M Terhal. *Ann. Phys.*, 326(4):839–866, 2011.
- [33] Isaac H. Kim. *arXiv preprint arXiv:1202.0052*, 2012.
- [34] Sergey Bravyi and Jeongwan Haah. *Phys. Rev. Lett.*, 111(20):200501, 2013.
- [35] Robert Raussendorf, Cihan Okay, Dong-Sheng Wang, David T. Stephen, and Hendrik Poulsen Nautrup. *Phys. Rev. Lett.*, 122(9):090501, 2019.
- [36] Trithap Devakul and Dominic J. Williamson. *Phys. Rev. A*, 98(2):022332, 2018.
- [37] David T. Stephen, Hendrik Poulsen Nautrup, Juan Bermejo-Vega, Jens Eisert, and Robert Raussendorf. *arXiv preprint arXiv:1806.08780*, 2018.
- [38] Michael Pretko. *Phys. Rev. B*, 95(11):115139, 2017.
- [39] Michael Pretko. *Phys. Rev. B*, 96(3):035119, 2017.
- [40] Kevin Slagle, Abhinav Prem, and Michael Pretko. *arXiv preprint arXiv:1807.00827*, 2018.
- [41] Daniel Bulmash and Maissam Barkeshli. *Phys. Rev. B*, 97(23):235112, 2018.
- [42] Han Ma, Ethan Lake, Xie Chen, and Michael Hermele. *Phys. Rev. B*, 95(24):245126, 2017.
- [43] Michael Pretko. *Phys. Rev. B*, 98(11):115134, 2018.
- [44] Michael Pretko. *Phys. Rev. D*, 96(2):024051, 2017.
- [45] Michael Pretko and Leo Radzihovsky. *Phys. Rev. Lett.*, 120(19):195301, 2018.
- [46] Andrey Gromov. *Phys. Rev. Lett.*, 122(7):076403, 2019.
- [47] Han Ma, Michael Hermele, and Xie Chen. *Phys. Rev. B*, 98(3):035111, 2018.
- [48] Han Yan. *Phys. Rev. B*, 99(15):155126, 2019.
- [49] Sagar Vijay. *arXiv preprint arXiv:1701.00762*, 2017.
- [50] Kevin Slagle, David Aasen, and Dominic Williamson. *SciPost Phys.*, 6(4):043, 2019.
- [51] Wilbur Shirley, Kevin Slagle, and Xie Chen. *SciPost Phys.*, 6(4):041, 2019.
- [52] Hao Song, Abhinav Prem, Sheng-Jie Huang, and Miguel Angel Martin-Delgado. *Phys. Rev. B*, 99(15):155118, 2019.
- [53] Daniel Bulmash and Maissam Barkeshli. *arXiv preprint arXiv:1905.05771*, 2019.
- [54] Cenke Xu and J. E. Moore. *Phys. Rev. Lett.*, 93(4):047003, 2004.
- [55] Cenke Xu and J. E. Moore. *Nucl. Phys. B*, 716(3):487–508, 2005.
- [56] Yizhi You, Trithap Devakul, F. J. Burnell, and S. L. Sondhi. *Phys. Rev. B*, 98(3):035112, 2018.
- [57] Han Yan. *arXiv preprint arXiv:1906.02305*, 2019.
- [58] G. K. Savvidy and F. J. Wegner. *Nucl. Phys. B*, 413(3):605–613, 1994.
- [59] George K. Savvidy. *arXiv preprint cond-mat/0003220*, 2000.
- [60] D. Espriu and A. Prats. *Phys. Rev. E*, 70(4):046117, 2004.
- [61] D. Espriu and A. Prats. *J. Phys. A: Math. Gen.*, 39(7):1743, 2006.
- [62] Kevin Slagle and Yong Baek Kim. *Phys. Rev. B*, 97(16):165106, 2018.
- [63] Wilbur Shirley, Kevin Slagle, Zhenghan Wang, and Xie Chen. *Phys. Rev. X*, 8(3):031051, 2018.
- [64] Abhinav Prem, Sheng-Jie Huang, Hao Song, and Michael Hermele. *Phys. Rev. X*, 9(2):021010, 2019.
- [65] J. P. Ibieta-Jimenez, M. Petrucci, and P. Teotonio-Sobrinho. *arXiv preprint arXiv:1907.01608*, 2019.